

Research papers

Simulation of thermal perturbation in groundwater caused by Borehole Heat Exchangers using an adapted CLN package of MODFLOW-USG



Matteo Antelmi ^{a,*}, Luca Alberti ^a, Sara Barbieri ^a, Sorab Panday ^{b,c}

^a Civil and Environmental Engineering Department, Politecnico di Milano, P.zza L. da Vinci 32, 20133 Milano, Italy

^b GSI Environmental Inc., Herndon, VA 20170, United States

^c Biological Systems Engineering Department, University of Nebraska-Lincoln, Lincoln, NE, United States

ARTICLE INFO

This manuscript was handled by Jiri Simunek, Editor-in-Chief, with the assistance of Giuseppe Brunetti, Associate Editor.

Keywords:
Borehole Heat Exchanger
CLN package
Modflow-USG
Unstructured grid
Groundwater
Heat Transport

ABSTRACT

Simulating heat transfer in an aquifer with one or more vertical Borehole Heat Exchangers (BHEs) of a Ground Source Heat Pump (GSHP) system by means of a finite difference code is difficult because of the square or rectangular geometry grid and computational times thus limiting the types of evaluations that can be performed. The aim of this work is to explore through MODFLOW-USG code (public domain software) a different approach towards simulating a borefield that would be more efficient computationally, in order to enable simulations of larger domains with multiple BHEs. The Connected Linear Network (CLN) package, introduced in MODFLOW-USG, generally simulates 1-D linear computational cells in a 3-D grid, such as hydraulic pipes in subsoil, but for the first time has been adapted to reproduce vertical closed loop U-pipe of a BHE. Therefore, this work evaluates the MODFLOW-USG and CLN package capability to reproduce the yearly operation of one or more BHEs in an aquifer as a simpler and faster approach compared to a very fine finite-difference discretization. Once the CLN package was adapted, a sensitivity analysis on the grid size refinement was performed. There were several findings from this work. The results of the different numerical models were in good agreement with an already validated model, in terms of exchanged energies and aquifer thermal perturbation. Same analyses were carried out for different groundwater flow velocities and it was confirmed that the exchanged energy by a BHE increases with the groundwater flow velocity in accordance with literature studies. At last, a borefield of 7 BHEs was implemented in a numerical model in a more expeditious and efficient way and without any computational effort.

1. Introduction

The thermal regime of aquifers underneath cities is a topic of increasing interest in recent years. It is related to the temperature variation of groundwater flow, that needs to be monitored in cities with low enthalpy geothermal systems or other anthropogenic forces (e.g., underground tunnels, sewage leaks or heating networks). Many authors studied how the groundwater temperature is influenced by climate change or anthropogenic forcers (Kupfersberger et al., 2017; Taylor and Stefan, 2009). Specifically, an increase of groundwater temperature affects the physical, biological and chemical properties of the aquifer (Hählein et al., 2013; Riedel, 2019), such as: aquifer-dependent organisms and ecosystems (Hancock et al., 2009), mixing processes of groundwater flow (Bonte et al., 2011) and silicates dissolution (Arning et al., 2006). Ground Source Heat Pumps (GSHP), using Borehole Heat

Exchangers (BHE) and Groundwater Heat Pumps (GWHP), using injection/extraction wells, are considered one of the main causes of the aquifer thermal perturbation (Ferguson and Woodbury, 2004; Menberg et al., 2013), even though this has not been adequately demonstrated (Lee and Hahn, 2006).

The influence of GSHP or GWHP systems on aquifers underneath cities was studied by several authors: Guimerà et al. (Guimerà et al., 2007) found out that, in several aquifers of European cities, abnormal effects in aquifer's temperature were probably caused by intensive use of the geothermal resource in the summer season. In summer, in Basel, Epting et al. (Epting et al., 2013) detected the maximum temperature of the aquifer right downstream of geothermal systems; in Zaragoza, Epting et al. (Epting et al., 2017) measured a groundwater temperature equal to 41 °C downstream of geothermal systems, compared to an average air temperature equal to 15.5 °C.

Whenever economic resources are not available for thermal

* Corresponding author.

E-mail addresses: matteo.antelmi@polimi.it (M. Antelmi), spanday@gsienv.com (S. Panday).

Nomenclature	
Symbol	Variable(Unit)
α, α_{MC}	Dispersivity, Dispersivity for the GWF-CLN interaction(m)
c_w, c_s	Specific heat capacity of water and soil(J/(kg·K))
ΔT	Temperature difference between inlet and outlet fluid of the BHE(K)
Γ_{MC}^*	Heat exchange term between soil matrix and CLN conduit (K/s)
h	Hydraulic head (m)
K	Hydraulic conductivity (m/s)
$\lambda_m, \lambda_{CLN}, \lambda_{MC}$	Effective thermal conductivity of the medium, along the length of the CLN domain, between the porous medium and the CLN conduit(W/(m·K))
L_{cc}, L_{MC}	Length dimension of the CLN cell, Hydraulic radius of the CLN plus the effective cell radius of the GWF cell (m)
m	Mass flow rate (kg/s)
n	Outward-pointing unit normal vector (-)
Q	Heat rate exchange (W)
q_b	Boundary heat flux (W/m ³)
ρ_b, ρ_w, ρ_s	Bulk density, water or soil density (kg/m ³)
S	Surface (m ²)
S_y, S_s	Specific yield, specific storage (m ⁻¹)
S_w	Saturation of water (-)
t	Time (s)
$T, T_s, T_{u,MC}, T_{in}, T_{out}, T_{MA}, T_{model}, T_{res}$	Temperature, Temperature of soil, Temperature of the upstream location between the matrix and the CLN cell, Temperature of the inlet/outlet fluid of the BHE, temperature of the model MA, Temperature of the model considered, Difference between T _{MA} and T _{model} (K)
V	Volume (m ³)
v_b, v_{cc}, v_{MC}	Darcy velocity in x_i direction, velocity of flow along the CLN cell, flux per unit area from CLN cell to GWF cell (m/s)
V_s	Fraction of the total volume of the CLN cell that is saturated (-)
ϕ	Porosity (-)
W	Volumetric source or sink per unit volume (s ⁻¹)

monitoring of the aquifer, a predictive analysis of the effects of GSHP and GWHP systems, by numerical modelling of flow and heat transport in aquifers, is the least invasive and most effective approach for evaluating the thermal impacts of BHE systems. Several scientific studies examined the problem of the heat transport in aquifers by means of analytical solutions (Alcaraz et al., 2016; Molina-Giraldo et al., 2011) or finite elements (Choi et al., 2011) or finite differences codes (Langevin et al., 2010; Somogyi et al., 2015). Among these solutions, common hydrogeological and hydrological software, such as MODFLOW (Harbaugh et al., 2000), MT3DMS (Zheng and Wang, 1999), FEFLOW (Diersch et al., 2010), HYDRUS (Šimůnek et al., 2016) are suitable for reproducing heat transfer between BHE and aquifer in different hydrogeological settings.

The MODFLOW/MT3DMS finite difference code, however, has limitations to reproduce several BHEs simultaneously in the same model because of the need of a very fine grid refinement. MODFLOW-USG (Panday et al., 2013) is the new version of the public domain software MODFLOW and is able to overcome these limitations, due to the use of an unstructured grid (Sbai, 2020) and the CLN package. The code has the potential of efficiently simulating large complex subsurface thermal regimes and their interaction with GSHP systems due to the unstructured grid capability that is effective for discretizing large domains at the appropriate resolution. Implementation of an unstructured formulation within the MODFLOW framework (MODFLOW-USG) allows application of regional models to address local problems (Feinstein et al., 2016). In addition to unstructured grids, MODFLOW-USG implements a CLN package of 1-D cylindrical cells that can be placed within a 3-D subsurface numerical grid. The CLNs readily implement specific features such as a closed-loop U-shape pipe (BHE), no longer requiring detailed grid refinement as in (Angelotti et al., 2014a).

Up to now many authors mainly used finite elements codes to implement one or more BHE in aquifers (Casasso and Sethi, 2019; Diersch et al., 2011a, 2011b; Piccinini et al., 2012). Al-Khoury et al. (Al-Khoury et al., 2010) implemented a double U-pipe BHEs in a finite element numerical model to simulate heat transfer with multiple BHEs in a numerically efficient manner. Bauer et al. (Bauer et al., 2011) developed and applied a 3D numerical simulation model for a U-shape pipe, implementing each element of the BHE (such as fluid inside well, grout etc.) with simplified thermal resistance and capacity models. Brunetti et al. (Brunetti et al., 2017) implemented a computationally efficient pseudo-3D model by means of HYDRUS, they validated it comparing the numerical results with a Thermal Response Test (TRT) data carried out at two different sites in Japan and at last used it to study

the influence of groundwater flow and geology on GSHP.

Success in numerical simulations of BHE systems in aquifers was followed by sensitivity studies that examined the impact and significance of hydrogeological and physical parameters (Casasso and Sethi, 2014). Many studies focused on thermal perturbations in the aquifer related to BHEs under different groundwater flow velocities (Angelotti et al., 2014b; Florea et al., 2017; Zanchini et al., 2012). Capozza et al. (2013) evaluated by means of analytical solutions (Moving Line Source) the effect of groundwater flow on the thermal drift in the aquifer, generated by the heating operation of a GSHP and evaluated the influence of an existing borefield on a nearby one, in presence of either still or moving groundwater.

The current paper compares the use of CLN package through the MODFLOW-USG code against the numerical solution proposed in (Angelotti et al., 2014a), for implementing BHEs and simulating the related thermal perturbation in groundwater. At first, a single BHE is implemented in a homogeneous aquifer and thermal and energy results are compared with Angelotti's model, that was already compared with experimental data (Antelmi, 2016) and was implemented using a classic finite difference grid refinement. Then MODFLOW-USG is applied to simultaneously simulate several BHEs to show how the CLN package can efficiently simulate the thermal perturbation in groundwater in a single numerical model faster and without computational efforts.

2. Material and methods

2.1. Groundwater flow modelling by means of MODFLOW-USG

MODFLOW-USG is a three-dimensional Control Volume Finite Difference (CVFD) groundwater flow modelling code first released in 2013 by the U.S. Geological Survey (Panday et al., 2013). The CVFD approach allows design of flexible structured or unstructured 3-D grids, represented by triangles, rectangles, hexagons, etc., to solve for the Groundwater Flow (GWF) process of the code. Furthermore, grids can include local nesting or other refinement methods. For example, quadtree refinement is another way to develop a nested grid with flexibility to add grid refinement only where needed (around a point, along a line, or within an area). The structural flexibility of the grid is a relevant issue when a numerical model needs to reproduce local problems in regional simulations such as the influence of rivers or wells, or to implement BHE or to discretize layers for better representations of hydro stratigraphic units.

The three-dimensional groundwater flow equation for the CVFD

formulation can be written as:

$$\int (K \nabla h) n dS = S_s V \frac{\partial h}{\partial t} + W V \quad (1)$$

where: K is hydraulic conductivity, h is hydraulic head, S_s is specific storage, V is the volume, t is time, W is a volumetric source or sink per unit volume, n is an outward-pointing unit normal vector on the surface (S) of the volume. Note that the integral of Equation (1) is a summation of flow between cells in a numerically discretized form. The formulation in MODFLOW-USG also accounts for unconfined conditions which are simulated based on the routines available in MODFLOW-2005 (Harbaugh, 2005) and MODFLOW-NWT (Niswonger et al., 2011). The Newton Raphson approach of MODFLOW-NWT provides for a robust, efficient, and stable solution methodology for simulating unconfined flow.

2.2. Connected linear network (CLN) process

A significant feature of MODFLOW-USG is the Connected Linear Network (CLN) Process to reproduce one-dimensional connection elements into a structured or unstructured three-dimensional GWF process grid (Panday et al., 2013). A one-dimensional CLN cell is a hydrogeologic or hydrologic water feature that has a cross-sectional dimension smaller than the longitudinal flow component of the feature, and the size of cell where is inserted. A CLN cell can reproduce wells, pipes, karst conduits, fractures, rivers, and many linear components that requires flow connections with the aquifer.

When a CLN element is implemented, a new domain is created; therefore, the distinction between the CLN domain (for CLN cells), and the groundwater domain (for GWF cells) is necessary; the CLN cell is separate from the GWF cell with flow possibly occurring between them (for instance, groundwater flow to a pumping well that is represented by a vertical cylindrical CLN cell). The introduction of a CLN component into the modelling domain is indeed equal to the introduction of a sub-model: a model inside the initial model; with its own nodal numbering and flow and transport equations solved in the CLN domain (and possibly interacting with the GWF domain). A strong capability of MODFLOW-USG is that the flow within the CLN and GWF domains and their interactions is solved fully implicitly within one matrix. Thus, the total number of cells in a model will be the sum of the number of CLN and GWF cells which have flow terms that are solved simultaneously.

Flow within the 1-D network of CLN cells includes laminar and turbulent flow formulations. Thus, flow within a CLN pipe occurs due to head gradients within it, against the resistance of the pipe or of fluid turbulence. The formulation is similar to Equation (1) for the GWF cell, except that storage of fluid within the hollow of the pipe, and the hydraulic conductivity is a function of the pipe flow formulation. Leakage formulations across the wetted circumference of the CLN tube, allow for interaction of water between CLN pipe and GWF cells. If necessary, the leakance can be set to a null value in order to reproduce impermeable tubes. Alternate formulations are also provided and they used analytical solutions to produce grid-independent solutions to flow between GWF and CLN domains thus allowing for small diameter wells to be properly simulated even within a large dimension GWF cell (Neville and Tonkin, 2004). Also, the CVFD formulation allows for a pipe spanning multiple groundwater cells, or for a network of multiple pipes to exist within a single groundwater cell since the flow is ruled by the connectivity and the area of flow between cells as noted in Equation (1). This flexibility is important in discretization of the domains appropriate to the flow characteristics within it, and one grid does not determine flexibility of another.

MODFLOW-USG applications commonly use CLNs to simulate pumping or abandoned wells within a groundwater domain. The CLN cells have also been used in a horizontal setting to simulate rivers and streams. Angled CLNs have been used to simulate karst features and CLNs have been used to represent multiple such features in one

simulation setting. What makes them ideal to simulate BHEs is that a few CLN cells can be joined in a U-Tube configuration, to simulate flow of fluids within the BHEs as well.

2.3. Heat transfer modelling

There have been several version updates and enhancements to MODFLOW-USG since its initial release in 2013. Several further developments have been published as open source and public domain USG-Transport software (Panday, 2020). It is also available in Groundwater Vistas 7 (GWF), which was used for pre-processing and post-processing of data and output for this study. Among the additional capabilities, the Block-Centered Transport (BCT) package has a crucial role in the current study because it implements solute (and heat) transport in a porous medium and in a CLN domain. The code solves for solute transport equations immediately after groundwater flow equations.

As already discussed in (Alberti et al., 2017; Thorne et al., 2006), the groundwater solute transport equation is comparable to the heat transport equation, therefore, the energy transport equation in groundwater can be written as:

$$\phi S_w \rho_w c_w \frac{\partial T}{\partial t} + (1 - \phi) \rho_s c_s \frac{\partial T_s}{\partial t} = \frac{\partial}{\partial x_i} \left[(\lambda_m \frac{\partial T}{\partial x_i} + \phi S_w \rho_w c_w \alpha v_i) \frac{\partial T}{\partial x_i} \right] - \frac{\partial}{\partial x_i} (\phi S_w \rho_w c_w v_i T) - \Gamma_{MC}^* + q_b \quad (2)$$

where: ϕ is the porosity, S_w the saturation of water, ρ_w and ρ_s the density of water and solid material, c_w and c_s the specific heat capacity of water and solid, T the temperature of water, t the time, T_s the solid temperature, λ_m the effective thermal conductivity of the medium, v_i the Darcy velocity in direction x_i , α the dispersivity, Γ_{MC}^* the heat exchange term between soil matrix and CLN conduit cell and q_b the boundary heat flux.

The energy conservation equation within the CLN domain (Equation (2)) can be written as:

$$\rho_w c_w \frac{\partial V_s T}{\partial t} = \frac{\partial}{\partial L_{cc}} \left[(\lambda_{CLN} + V_s \rho_w c_w \alpha v_{cc}) \frac{\partial T}{\partial L_{cc}} \right] - \frac{\partial (\rho_w c_w v_{cc} T)}{\partial L_{cc}} + \Gamma_{MC}^* + q_b \quad (3)$$

where: V_s is the fraction of the total volume of the CLN cell that is saturated during unconfined conditions, L_{cc} is the length dimension of the CLN cell, λ_{CLN} is the thermal conductivity along the length of the CLN domain, and v_{cc} is the velocity of flow along the CLN cell. Note that a CLN cell can be vertical, horizontal, or angled.

Equation (3) for heat transfer in the CLN domain is similar to Equation (2) for energy transport in the groundwater domain, except that heat flow equation is 1-D along the length of the CLN pipe instead of 3-D in the subsurface. Also, in Equation (3), the heat capacity of CLN pipe is neglected (only of water within the pipe is included) and therefore an adsorption type term is not included. Furthermore, as the heat conductance along the CLN material is neglected, then the effective CLN heat conductance can be expressed only by the liquid phase conductance, as follows:

$$\lambda_{CLN} = V_s \lambda_w \quad (4)$$

Note that the term Γ_{MC}^* appears with a negative sign in Equation (2) but a positive sign in Equation (3) because heat lost from the GWF domain will equal the heat gained by the CLN domain. This heat transfer occurs due to advection and dispersion and is expressed as:

$$\Gamma_{MC}^* = - \frac{\partial (v_{MC} T_{u,MC})}{\partial L_{MC}} + \frac{\partial}{\partial L_{MC}} \left[(\alpha_{MC} v_{MC} + V_s \lambda_{MC}) \frac{\partial T}{\partial L_{MC}} \right] \quad (5)$$

where: v_{MC} is the flux per unit area from CLN cell to GWF cell representing convective flux of heat between CLN and GWF domain, $T_{u,MC}$ is the temperature of the upstream location between the matrix and the CLN cell, L_{MC} is the hydraulic radius of the CLN cell plus the effective cell

radius of the GWF cell and λ_{MC} is the thermal conductivity between the porous matrix and the fluid within the CLN pipe. The first term on the right side of Equation (5) represents advective heat transfer and the second term represents dispersive heat transfer. But for closed BHE systems, there is no interaction of fluids between the BHE pipe and the external groundwater and thus ν_{MC} will be zero (the leakance between GWF and CLNs can be set to zero while solving for flow to simulate the closed BHE system). For that case, only the heat conductivity term between CLN and GWF domains transfers energy between the domains (i.e. no fluid transfer between the domains).

MODFLOW-USG code, coupled with CLN process, does not yet include convective heat transfer coefficient, which is considered relevant in the energy exchange performed by the BHE and in groundwater temperatures close to the BHE. Nevertheless, this study mainly focuses on environmental impacts of BHE and on groundwater temperatures from 2 m up to 30 m downstream of the BHE, where the convective heat transfer coefficient seems to represent a subdued percentage of the total energy exchanged with groundwater, as explained in Numerical results and discussion section. MODFLOW-USG solves the energy transport equation in a fully implicit manner, similar to the flow equation solution between domains. Thus, energy transport within the GWF domain (Equation (3)), energy transport within the CLN domain (Equation (4)), and energy transfer between domains (Equation (5)) are all assembled into one matrix for solution of the entire system at each time step. Boundary conditions can then be provided to the GWF domain to simulate appropriate heat transfer into groundwater, for example from/to rivers, recharge, evapotranspiration, wells, etc. Those boundaries can be provided with a prescribed temperature condition or a prescribed heat flux condition (with inflowing or outflowing water). Specifically, for the BHE implementation a boundary conditions needs to be provided

to cells of a CLN tube to represent the heat input and output of the BHE: a prescribed inflow temperature and inlet flow rate (Neumann condition) should be assigned to the inlet CLN node whereas just a constant flow rate have to be assigned to the outlet CLN node.

The representation of the BHE in the numerical model and the connections between GWF or CLN nodes and boundary conditions is summarized in the Fig. 1.

2.4. Numerical model: Implementation of the BHE

The implementation of a BHE in finite different codes was up to now quite complex. The main limitation was the reproduction of circular geometries in codes such as MODFLOW, which use rectangular or square grids. As discussed in (Angelotti et al., 2014a), a very strong grid refinement was necessary (Fig. 2a) to validate the numerical model of a BHE related to analytical solutions.

In (Angelotti et al., 2014a) through MODFLOW/MT3DMS, the BHE was implemented as: one U-shape pipe, where the heat carrier fluid flows vertically by means of 36 cells, enclosed within 0.37 cm cells, reproducing polyethylene (grey cells in Fig. 2a), a horizontal pipe section at the bottom of the BHE to join the two pipes, (Angelotti et al., 2014a) and 3 vertical layers (ranging in thickness from 0.37 to 3.36 cm). For other details, please see the publication of (Angelotti et al., 2014a).

Using MODFLOW-USG, the BHE was implemented by means of two analytical elements named "CLN Well" and one named "CLN polyline" (Fig. 2b). The "CLN Well" is a vertical conduit consisting of CLN cells placed in all layers of the discretized 3-D GWF domain and used to reproduce the vertical inlet and outlet pipes of the U-tube. Wells have circular geometry therefore they reproduce a real BHE more closely than the square section used in the MODFLOW/MT3DMS model of (Angelotti

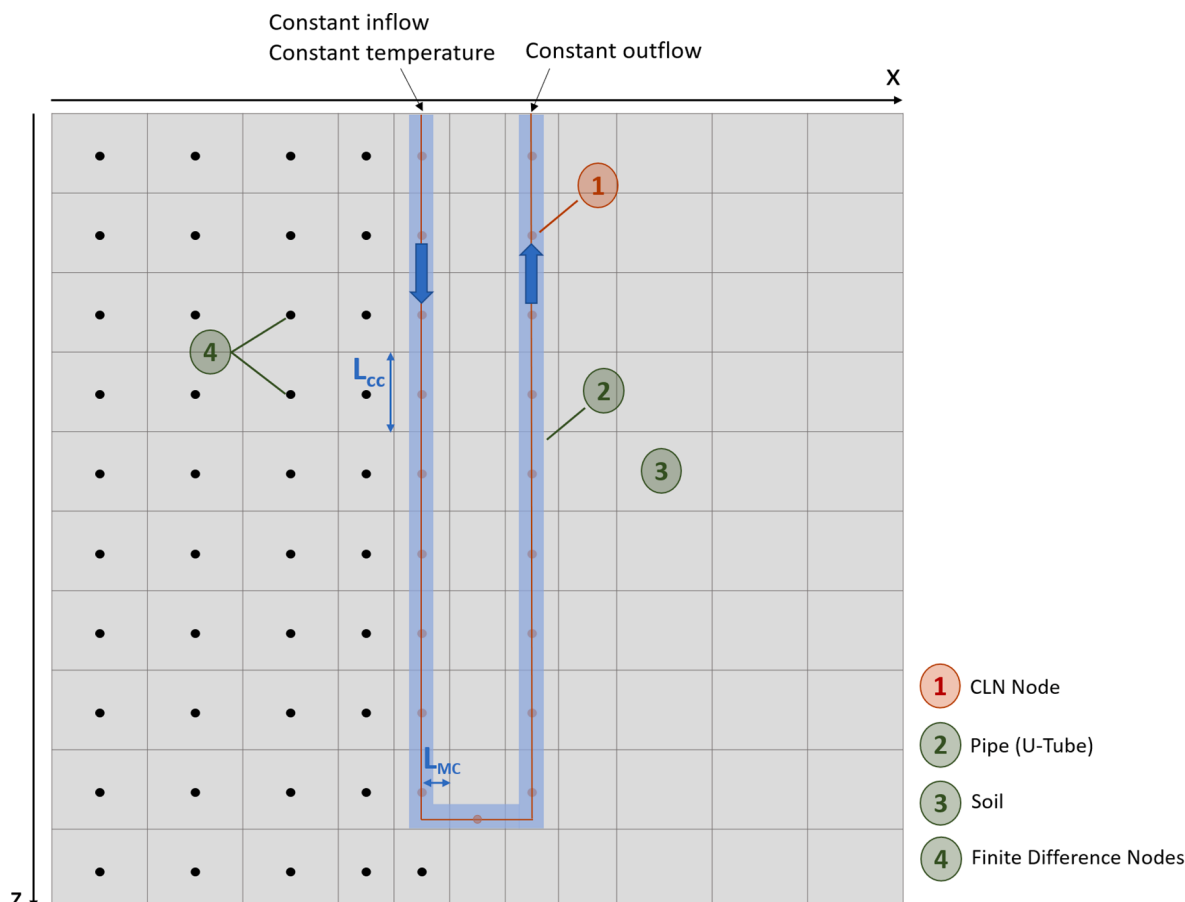


Fig. 1. BHE representation within the model domain.

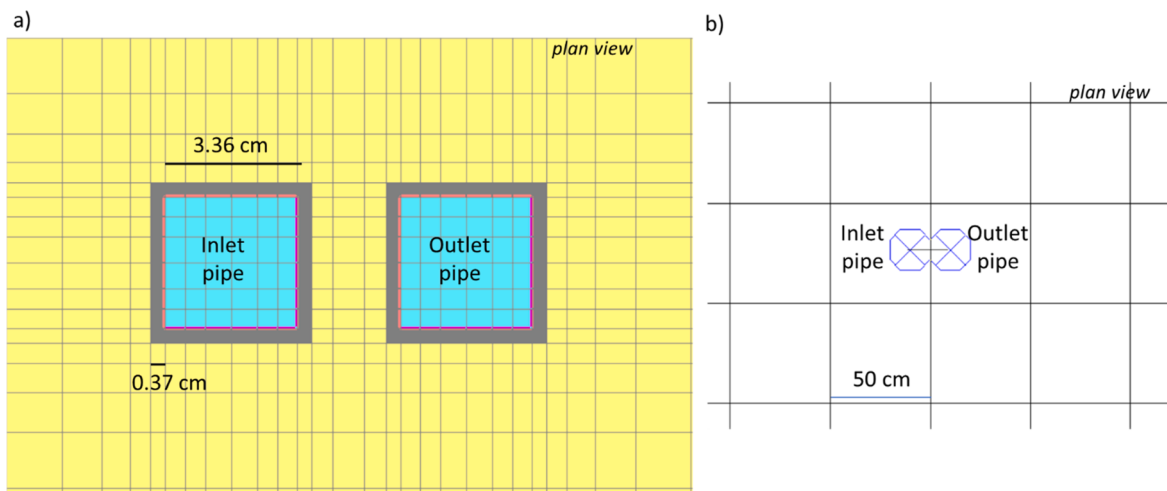


Fig. 2. Representation of the BHE (a) in MODFLOW/MT3DMS (Angelotti et al., 2014a) and (b) in MODFLOW-USG using two “CLN Well” and one “CLN polyline”.

et al., 2014a). The horizontal section of the BHE, connecting outlet to inlet U-pipe, was implemented by means of the analytical element “CLN polyline”, generally used for horizontal hydraulic pipes.

The ensemble of the three CLN elements ensures the continuous circulation of the heat carrier fluid inside the U-pipe. Instead of assigning constant head boundary conditions to inlet/outlet of the U-pipe to reproduce the circulation as in (Angelotti et al., 2014a), users need only to insert the flow rate within the U-pipe (here, 1000 kg/h). At the top of the inlet U-pipe, a constant temperature value (depending on the heating or cooling period, as shown in Table 1) was assigned modifying the Prescribed Concentration Boundary (PCB) package, that is generally used to implement constant concentration boundary conditions (Barbieri, 2020). In (Angelotti et al., 2014a), the numerical simulations were run imposing a constant heat rate (reproducing TRT, such as in (Brunetti et al., 2017)) or a constant input temperature at the inlet pipe of the BHE (reproducing the typical yearly operation of a GSHP), whereas in the present study MODFLOW-USG simulations were run only to reproduce the typical GSHP yearly operation (Table 1).

The case study implemented in MODFLOW-USG refers to a typical BHE, consisting of a 100 m polyethylene U-pipe with an inner radius of 2 cm and a pipe-to-pipe centers distance of 8 cm. The U-pipe is located into a 160 m saturated homogenous and not dispersive sandy aquifer. For the sake of simplicity, the borehole filling material (grout) is assumed to be equal to the surrounding soil. The aquifer has an initial unperturbed uniform temperature of 11.8 °C, representative of the yearly average outdoor temperature in North Italy. Hydrogeological and physical properties representing the aquifer were assigned to active cells using the same values implemented in (Angelotti et al., 2014a) and are shown in Table 2. All the MODFLOW-USG models were compared to the Angelotti model with a groundwater Darcy velocity of 10^{-5} m/s, in following pages named “MA”.

In addition, different groundwater velocities were also implemented by varying the hydraulic conductivity. Constant head (100 m) and constant unperturbed temperature (11.8 °C) boundary conditions were assigned to the left side of the model domain while only constant head (99.5 m) was assigned to the right one (blue cells in Fig. 3), for a constant hydraulic gradient equal to 0.005. Initial temperature of 11.8 °C

Table 2

Hydrogeological and physical properties implemented in MODFLOW-USG and received from (Angelotti et al., 2014a).

Parameter	Value	Measurement Unit
Hydraulic gradient, i	0.005	–
Aquifer horizontal hydraulic conductivity, K_x	0.002	m/s
Aquifer vertical hydraulic conductivity, K_z	0.0002	m/s
BHE hydraulic conductivity, K_{BHE}	11.5	m/s
HDPE hydraulic conductivity, K_{HDPE}	10^{-21}	m/s
Aquifer porosity, ϕ	0.35	–
Aquifer Specific Yield, S_y	0.2	–
Aquifer Specific Storage, S_s	0.01	m^{-1}
Bulk density, ρ_b	1700	kg/m^3
Aquifer heat conductivity, λ_m	2.28	$W/(m \cdot K)$
Thermal diffusion coefficient, D^*	$1.56 \cdot 10^{-6}$	m^2/s
Aquifer heat capacity, c_s	753.5	$J/(kg \cdot K)$
Thermal distribution coefficient, K_d	$1.8 \cdot 10^{-4}$	m^3/kg

was set to the entire model domain.

The model domain is 100 m long and 50 m wide and according to the different grid refinement (Table 3), a different number of cells was adopted varying from 80,432 to 375536. For each model, the vertical domain was discretized into 16 layers with a constant thickness equal to 10 m, for an aquifer depth of 160 m and the properties are always the same reported in Table 2.

2.5. Numerical model: Grid refinement

To test the impact of grid resolution on the results, different numerical models, implementing different grid refinement solutions were compared with the (Angelotti et al., 2014a), as shown in Table 3 and Fig. 4.

The “CLN_QT1”, “CLN_QT2” and “CLN_QT3” models were implemented using a quadtree refinement located around the BHE respectively with a minimum cell size ranging from 5 to 50 cm; otherwise, the “CLN_1”, “CLN_2” and “CLN_3” models were implemented using a classic refinement (similar to the “MA” model), with a minimum cell size again ranging from 5 to 50 cm.

The “quadtree” refinement is performed by division of the study area in different zones, which correspond to the zones with different cells size or refinement (smaller cells are in higher numbered zones): a maximum of 7 zones can be defined and the zone number 1 is the area where the cells are not divided, zone 2 is the area where each cell is divided in 4 cells, zone 3 is the area where each cell is divided in 16 cells and so on up to zone 7.

In each model the two analytical elements “CLN Well”, described

Table 1
Stress period length and inlet pipe temperature implemented in numerical model.

GSHP operation	Heating	Pause	Cooling	Pause
Time (d)	180	50	90	40
Temperature (°C)	1	–	28	–

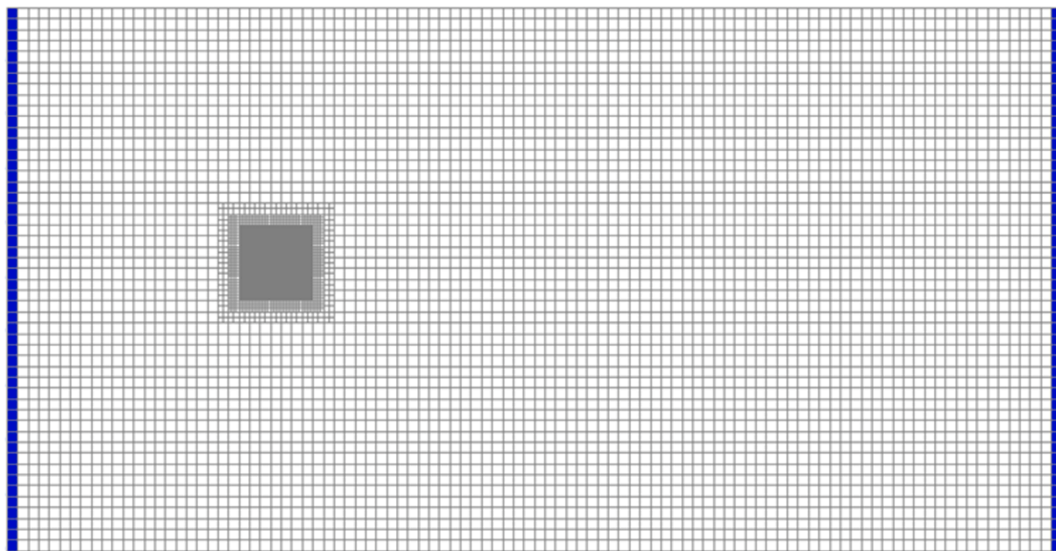


Fig. 3. Plan view of the numerical model domain.

Table 3
Numerical models implemented in MODFLOW-USG.

Numerical model	Features	Minimum cell size (cm)
MA	Model validated in (Angelotti et al., 2014a) without CLN package	0.37
CLN_QT1	Model with CLN and quadtree refinement	6
CLN_QT2	Model with CLN and quadtree refinement	25
CLN_QT3	Model with CLN and quadtree refinement	50
CLN_1	Model with CLN and without quadtree refinement	5
CLN_2	Model with CLN and without quadtree refinement	20
CLN_3	Model with CLN and without quadtree refinement	50

above, were inserted in two adjacent cells, which dimensions are shown in Table 3 for each model. The two “CLN Well” elements (interconnected at layer 10 by “CLN polyline”) were always horizontally inserted at the same distance (8 cm) and vertically from layer 1 to layer 10.

To compare the results of the new models to the “MA” model, an absolute residual value of temperature was calculated as the absolute value of the difference between the temperature achieved in the “MA” model and the temperature in new models. The residual values were calculated at 4 different times (t , one for each operation period) or at certain distances (d) for observation points downstream of the BHE, with the following formulations:

$$T_{res}(t) = T_{MA}(t) - T_{model}(t) \quad (6)$$

$$T_{res}(d) = T_{MA}(d) - T_{model}(d) \quad (7)$$

Where T_{res} is the difference between the temperature achieved in “MA” model (T_{MA}) and the temperature achieved in new models (T_{model}) reported in Table 3.

3. Numerical results and discussion

In this section the results of the heat transport numerical simulations are discussed showing the comparison between “MA” model and “CLN” models varying the grid refinement and the Darcy velocities and the

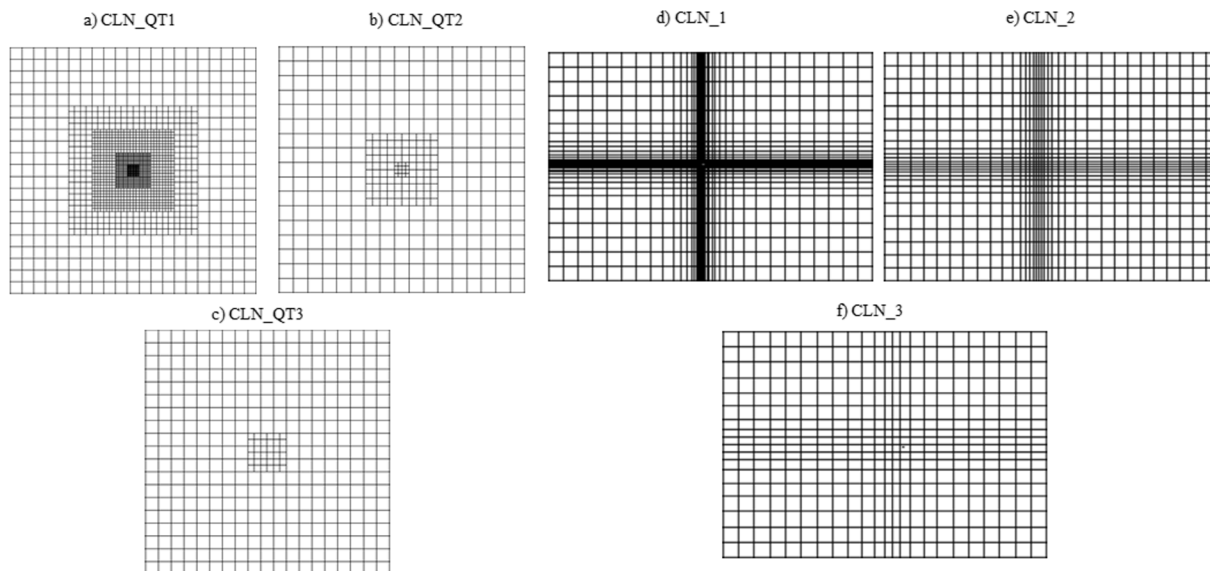


Fig. 4. Plan view of the grid refinement in the 6 numerical models implemented.

number of BHE in a borefield. Once the model with one BHE was validated, other models were implemented to reproduce more than one BHE in the same modelling domain.

3.1. Grid refinement

3.1.1. Heat carrier fluid temperature at the outlet pipe of the BHE

The outlet temperatures of the heat carrier fluid circulating inside the BHE are shown only for the winter season after 180 days of simulation in Table 4. These values reproduce the temperature value of the fluid at the last outlet section pipe of the BHE, regardless of the temperature distribution along the entire depth of the BHE.

The outlet fluid temperatures are in accordance with the "MA" model up to 11%. Considering that both the results of the "MA" model were validated with respect to analytical solutions showing 10% variation and were compared with experimental data (Antelmi et al., 2020; Ly, 2015), the differences achieved are similar, therefore they showed good accordance. "CLN_QT3" and "CLN_3" models, respectively a quadtree and classical refinement with a minimum cell size of 50 cm, showed the best fit when compared to "MA model".

The "MA" model showed more problems to reach convergence; specifically, one run took a long time to reach the final solution and, moreover, before the run, a lot of time and effort was spent to find the right set of solver parameters in MT3DMS that allowed convergence of the solution. Differently, the MODFLOW-USG models did not have convergence issues, did not need to find convergence parameters, and ran quickly.

3.1.2. Energy exchanged by the BHE

A further comparison, related to the outlet fluid temperatures, was based on the exchanged energy between the BHE and the aquifer, calculated from the heat rate exchanged (Q) in each Time Step:

$$Q = m \cdot c_w \cdot (T_{in} - T_{out}) \quad (8)$$

Where: m is the mass flow rate circulating in the BHE, T_{in} is the BHE fluid inlet temperature and T_{out} is the fluid outlet temperature.

The simulations last 180 day for heating period (inlet fluid temperature equal to 1 °C) and 90 days for cooling period (inlet fluid temperature equal to 28 °C). After a few days the heat rate values reached a steady-state condition because of the significant groundwater velocity (10^{-5} m/s). The energy exchange, that is the integral underlying the heat rate curve Q for specific time period, was calculated for both winter and summer season and shown in Table 5.

From the Table 5, each model showed a higher energy exchange in winter season than in summer because of the initial hypothesis of stress periods length (Table 1). The differences between "MA" model and remaining models are equal in winter and summer seasons. The difference between "MA" model and "CLN" models was less than 13%. Specifically, for the cooling season, maximum difference was achieved for "CLN_QT1" (classic refinement and cell size of 6 cm) and for "CLN_1" (quadtree refinement and cell size of 5 cm), respectively equal to -11 and -12.9%. These differences agreed with the outlet fluid temperatures and were considered acceptable.

Table 4

Heat carrier fluid temperature at the outlet pipe after 180 days.

Model	T_{out} (°C)	Difference with "MA" model (%)
MA	5.83	
CLN_QT1	5.30	-9
CLN_QT2	6.23	7
CLN_QT3	5.72	-2
CLN_1	5.21	-11
CLN_2	6.22	7
CLN_3	5.59	4

Table 5

Exchanged energies by the BHE for the heating and cooling periods.

Model	$E_{heating}$ (kWh)	% difference with "MA" model	$E_{cooling}$ (kWh)	% difference with "MA" model
MA	23,996	-	17,991	-
CLN_QT1	21,371	-10.9	16,008	-11.0
CLN_QT2	26,004	8.4	19,483	8.3
CLN_QT3	23,462	-2.2	17,578	-2.3
CLN_1	20,933	-12.8	15,676	-12.9
CLN_2	25,932	8.1	19,425	8.0
CLN_3	22,831	-4.9	17,106	-4.9

3.1.3. Temperature in the aquifer

Groundwater temperatures of an observation well located at 5 m downstream of the BHE were monitored for a period of one year in each layer. Since the aquifer is sandy homogeneous, temperatures along the depth varied less than 0.1 °C, therefore a medium depth, corresponding to layer 5 (45 m depth), was chosen as the most representative of the vertical profile (Fig. 5).

In each model, during winter or summer season, the temperature reached an equilibrium value after a few days. Similarly, during the pauses, the undisturbed value of the aquifer temperature (11.8 °C) was rapidly reached. This is due to the advection phenomenon, that ruled the heat transfer in these simulations. In Fig. 5, "MA" model reached a temperature value equal to 11.2 °C during the heating period and 12.8 °C during the cooling period of the GSHP.

In Table 6, the absolute residual values of temperature compared to the "MA" model were calculated at the observation point (5 m downstream of the BHE) as in Equation (6) at 4 different times, one for each simulation period (winter, spring, summer and autumn seasons).

The absolute residual temperature showed a good agreement between "MA" model and new models: during heating period ($t = 109$ d) or during cooling period ($t = 249$ d), the worst temperature differences were respectively less than 0.16 °C and 0.24 °C; during the pause, the differences become negligible. In summary, in this observation point, the difference between "MA" model and new models was always less than 0.25 °C, therefore the ability of each new model to reproduce groundwater temperatures similar to the MA model was clear.

Further checks were carried out on the groundwater temperature for a specific time (at the end of the heating period) along distance downstream of the BHE. As above, the groundwater temperature values refer to layer 5 at 8 different observation points located into the domain for a distance from BHE ranging from 5 cm to 10 m (Fig. 6).

From Fig. 6, "CLN_QT1" and "CLN_1" model showed temperatures closest to the "MA" model. On the other hand, models less discretized ("CLN_QT2", "CLN_2", "CLN_QT3" and "CLN_3") showed high temperature values around the BHE, despite similar results to "MA" model in terms of outlet fluid temperature and exchanged energies. This is what it was expected because the implementation of the CLN package is comparable to a sub-model inside another model, where CLN cells are connected to GWF cells by means of the equation (5). Grid resolution was therefore significant in the evaluation of temperature around the BHE; for instance, between the BHE and 50 cm downstream of it, "CLN_QT3" model has only one groundwater temperature value (i.e. one node), "CLN_QT2" has 2 values, "CLN_QT1" has 9 values due to the larger number of cells. Same explanation can be given for "CLN_1", "CLN_2" and "CLN_3" models.

In Table 7, the absolute residual values of temperature were calculated for the same observation points at the same time as in Equation (7), equal to the end of the heating period.

Table 7 shows higher absolute residual values of temperature in the proximity of the BHE (0.05 m and 0.24 m) and especially in the "CLN_QT3" and "CLN_3 models", due to their coarse spatial discretization. From the distance of 5 m downstream of the BHE (typical value of interaxle spacing between adjacent BHEs in a borefield), the maximum temperature difference between the validated model and new models is

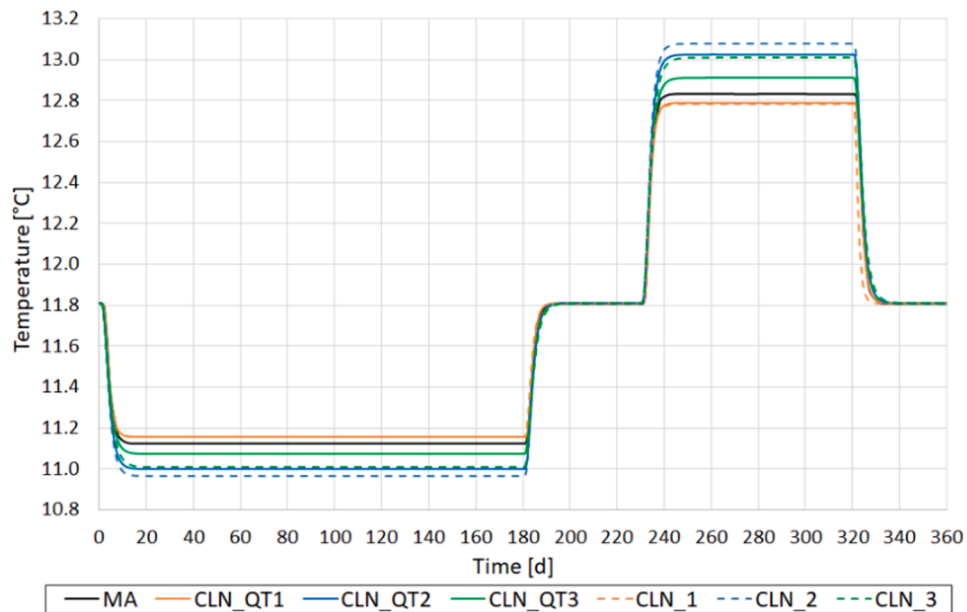


Fig. 5. Groundwater temperatures over time, at layer 5, in one monitoring well located 5 m downstream of the BHE observed in model MA (black line), CLN_QT1 and CLN_1 (orange lines), CLN_QT2 and CLN_2 (blue lines), CLN_QT3 and CLN_3 (green lines). (For interpretation of the references to colour in this figure legend, the reader is referred to the web version of this article.)

Table 6

Absolute residual temperature [°C] at 4 times instants (days) in layer 5, at observation point located 5 m downstream from the BHE.

Season	t (d)	T _{res} (t) (°C) CLN_QT1	CLN_QT2	CLN_QT3	CLN_1	CLN_2	CLN_3
winter	109	0.03	0.13	0.05	0.03	0.16	0.12
pause	219	1.2E-03	1.4E-04	4.3E-04	8.6E-04	2.7E-05	8.9E-05
summer	249	0.05	0.19	0.08	0.05	0.24	0.17
pause	324	0.01	0.10	0.07	0.30	0.06	0.11

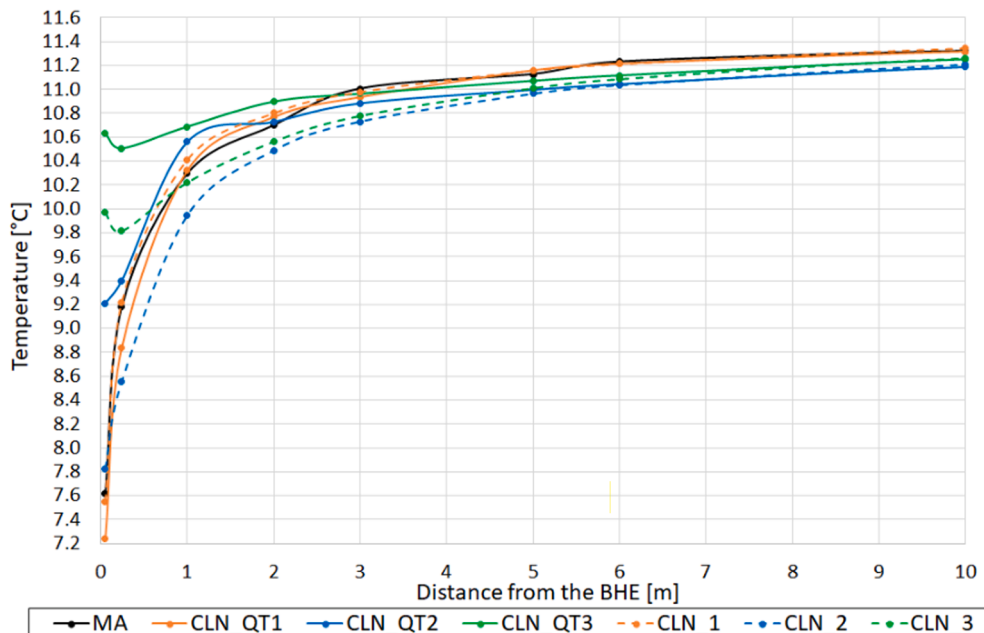


Fig. 6. Groundwater temperatures at 180 days, layer 5, in different monitoring points downstream of the BHE.

equal to 0.16 °C. Therefore, the adaptation performed on the CLN package is adequate to numerically simulate the heat transfer in aquifer. As previously discussed, the CLN approach does not consider the

convective heat transfer coefficient, but on the opposite, it was accounted in the “MA” model, which represented through 36 cells the water flowing into the pipe. Nevertheless, considering the domain

Table 7

Absolute temperatures residues [°C] calculated at $t = 180$ days in layer 5 at 8 locations downstream of the BHE compared to MA model.

d (m)	T _{res} (d) (°C)					
	CLN_QT1	CLN_QT2	CLN_QT3	CLN_1	CLN_2	CLN_3
0.05	0.38	1.60	3.01	0.06	0.21	2.35
0.24	0.34	0.22	1.33	0.04	0.63	0.63
1	0.02	0.27	0.39	0.12	0.35	0.07
2	0.07	0.03	0.20	0.10	0.21	0.14
3	0.07	0.12	0.04	0.03	0.27	0.23
5	0.03	0.13	0.05	0.03	0.16	0.12
6	0.02	0.18	0.11	0.02	0.20	0.15
10	0.01	0.13	0.07	0.03	0.11	0.06

beyond 2 m from the BHE, as the above results show, each MODFLOW-USG model simulates groundwater temperatures very close to the one simulated in the “MA” validated model. Therefore, when the simulations aim is the environmental impact, neglecting the convective heat transfer coefficient does not lead to wrong results. Differently, the discrepancy in energy and temperatures close to the BHE results are more relevant and when the simulations aim is the evaluation of the BHE energy performances, indeed that mechanism should be considered.

3.2. Darcy velocities

Further efforts were conducted on the quadtree refinement models (“CLN_QT1”, “CLN_QT2” and “CLN_QT3”) varying the hydraulic conductivity values. So, considering the Darcy velocity as product of hydraulic conductivity and hydraulic gradient, it ranged from a maximum of 10^{-4} m/s to minimum of 10^{-6} m/s. The aim was to evaluate how the heat transfer changed when the advection term varied, such as in (Angelotti et al., 2014a). The results were compared in terms of groundwater temperature (Fig. 7) and exchanged energy between BHE and aquifer at the end of the heating period. The groundwater temperatures in the case of Darcy velocity equal to 10^{-5} m/s corresponds to the “MA” model and was reported in previous Fig. 6.

Examining the results at the end of the heating period, when the groundwater flow velocity increased, the cold thermal plume moved faster downstream of the BHE: in Fig. 7 (a) the groundwater temperatures were highest in the proximity of the BHE, with a minimum value of 9.3 °C corresponding to “CLN_QT1” model. When the groundwater flow velocity was lower (10^{-6} m/s) the thermal plume moved slowly and lower values (up to 5.5 °C), corresponding to “CLN_QT1” model, were achieved close to the BHE (Fig. 7 b). This result is confirmed by the prevalence of the advection term: when groundwater flow is high, the water coming from upstream (with an undisturbed temperature equal to

11.8 °C) washed away the cold plume stretching it and groundwater temperatures result closer to the undisturbed temperature value. For the 3 velocities CLN_QT1 showed temperatures closest to the “MA” model confirming that a high grid refinement is able to give better results throughout the domain. On the other hand, the coarser grids gave larger errors closer to the BHE and mainly for highest velocities than for lower ones (Fig. 7 b). Generally, it is possible to affirm that the “CLN_QT1”, “CLN_QT2” and “CLN_QT3” models were in accordance with the “MA” model, as after 5 m downstream the BHE, the temperature difference result less than 0.25 °C, as seen for the groundwater flow velocity equal to 10^{-5} m/s.

The results of the exchanged energy showed the same results discussed in (Angelotti et al., 2014a), where, as the groundwater velocity increased, the energy performance of GSHP system proportionally increased for each new model, regardless of the spatial discretization used.

3.3. Application to a borefield of 7 BHE

Finally, the 3 models above described implementing CLN package and quadtree refinement, were used to simulate 7 BHEs at the same time. Here the intention was to show the potentialities of the new way to represent BHE by means of CLN elements and quadtree and to evaluate BHEs overlapping effects. The area, where the quadtree refinement was applied, was extended because of the presence at the 7 BHEs as noted on Fig. 8. The BHEs properties are the same as the previous models. The distance between each BHE was equal to 7 m and they were located parallel to the groundwater flow direction. This choice allowed examination of overlapping thermal plumes and evaluation of the groundwater temperature distribution in several downgradient observation points. The Darcy velocity was equal to 10^{-5} m/s.

The numerical simulations were performed assuming a heating operation of 180 days with a constant inlet fluid temperature (1 °C). Fig. 9 shows the groundwater temperature distribution downstream of the 7 BHEs (layer 5) at the end of the simulation.

Comparing Fig. 6 and 9, the temperatures in the proximity of the BHEs are lower than the same model where only one BHE was present in the domain: for instance, in the new simulations groundwater temperatures of the “CLN_QT1” model ranged from a minimum of 6.5 °C (at 5 cm downstream of the 7th BHE) to a maximum of 10.4 °C (at 10 m downstream of the 7th BHE), whereas in the model representing one BHE groundwater temperatures were higher ranging from 7.2 °C to 11.2 °C. Similar behavior can be observed for the CLN_QT2 and CLN_QT3 cases. This is due to the overlapping effects created by the GSHP heating operation. The effect of the overlapping is also clearly showed by the analysis of the exchanged energies. During the heating

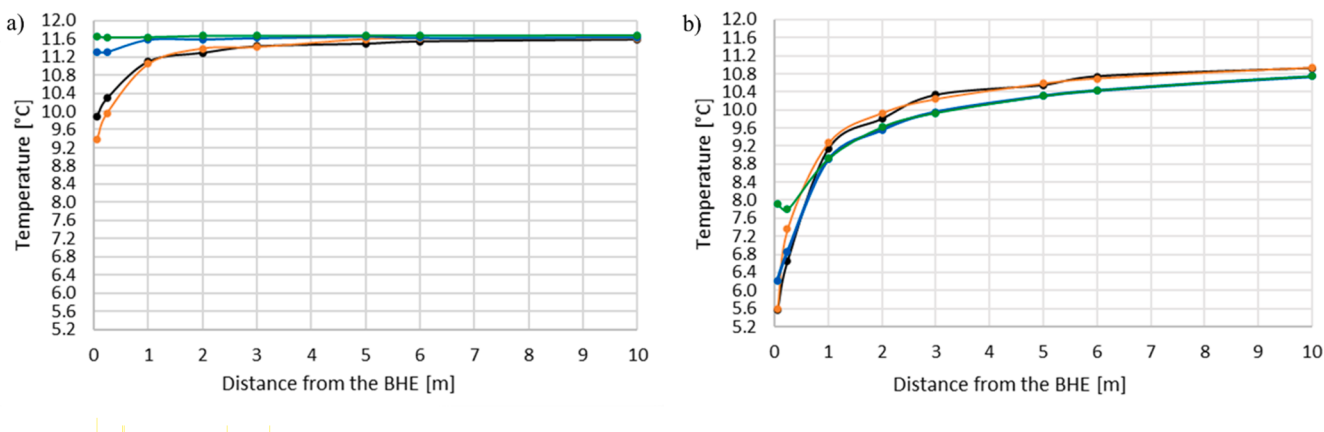


Fig. 7. Groundwater temperature at 180 days, layer 5, in different monitoring points downstream of the BHE observed a) Darcy velocity equal to 10^{-4} m/s; b) Darcy velocity equal to 10^{-6} m/s. For darcy velocity 10^{-5} m/s, minimum temperature for CLN_QT1 was 7.2

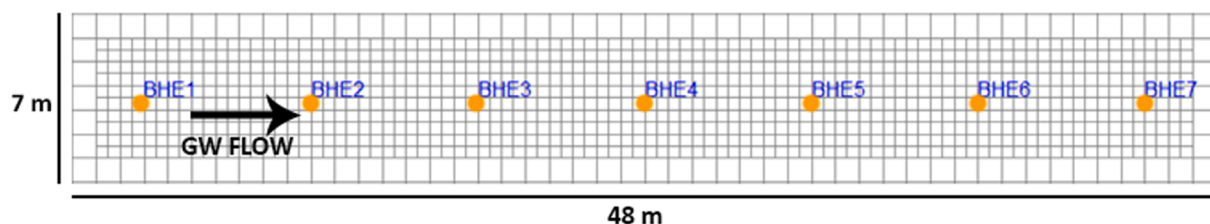


Fig. 8. Detail of the modelling domain in the surrounding of the 7 BHEs.

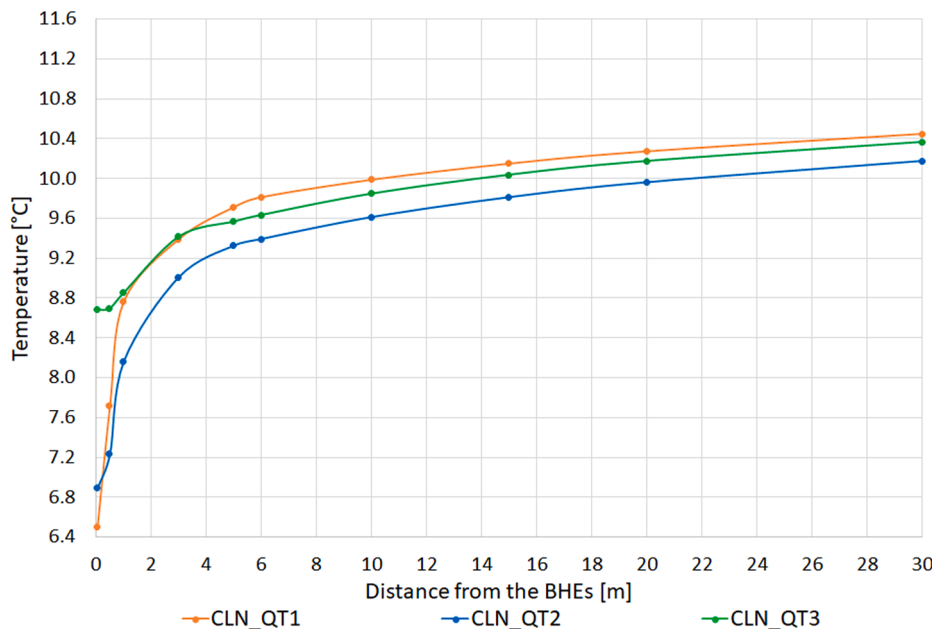


Fig. 9. Groundwater temperatures at 180 days, layer 5, at different monitoring points downstream of 7th BHE for 3 different type of quadtree refinement.

period, the energy exchanged by the BHE 7, that is influenced by the six cold plumes flowing from the upstream exchangers, ranges from 16 to 19% lower than the BHE 1 depending on the grid discretization implemented in the considered numerical model.

The numerical simulations showed the great advantage of simulating simultaneously more than one BHE in a unique numerical model, to evaluate the impact of implementation of one or more geothermal probes on groundwater and on each other. This is possible by adapting the CLN package and using special grid refinement. No comparison with “MA” model was carried out because to reproduce more than one BHE with a strong grid refinement was not practical and quite impossible for the numerical burden.

4. Conclusions

Evaluation of the thermal perturbation of aquifers in cities is an interesting and practical theme: the comprehension of the anthropogenic forcing able to alter the unperturbed thermal regime of a city's aquifer is essential. This study explains how to implement BHE in an aquifer by means of the finite difference code (MODFLOW-USG) in a more efficient, innovative and quick way compared to the classic MODFLOW/MT3D approach. The proposed methodology involves the use of vertical and horizontal CLN elements to reproduce the U-pipe of a real BHE.

To verify proper operation of the BHE system in an aquifer as represented by the CLN package, different numerical models were implemented varying the spatial grid discretization around the BHE: three numerical models were implemented by means of a new grid refinement method (quadtree refinement) available in MODFLOW-USG and three

models were implemented by means of a classical refinement method. The minimum cell dimension, where the BHE was located, ranged from 5 cm to 50 cm.

The results of the new numerical simulations were compared to the “MA” model (Angelotti et al., 2014a) implemented in MODFLOW/MT3DMS and previously validated through the comparison with an analytical solution. Comparing the temperatures of the heat carrier fluid at the outlet pipe, the difference between the “CLN” models and the “MA” model was less than 0.6 °C; in terms of exchanged energies, the difference was less than 13%. Groundwater temperatures at distances greater than 5 m downstream of the BHE show differences between new models and “MA” model of less than 0.25 °C. Some refined grid configurations were closest to the results of the “MA” model, including the case with a cell size of 50 cm. Such a configuration is the right compromise because it is closer to the validated model “MA” and is easily implementable into practical models without strong grid refinement. Other simulations were performed varying the groundwater flow velocity and the results achieved were very similar to the “MA” model: a strong increase in energy performance and a lower thermal disturbance in terms of absolute groundwater temperature values was noted as velocity increases.

The new approach with the CLN package and quadtree refinement in MODFLOW-USG, unlike the conventional methodology of other finite difference codes, shows the ability to simultaneously simulate more than one BHE in an aquifer in a single heat transport numerical model. This could provide the GSHP system designer additional insights resulting from the modeling of heat transfer in the aquifer and the evaluation of BHE interferences. In addition, by means of predictive modelling scenarios, environmental consultants will also be able to estimate the

contribution of different GSHP systems in total aquifer thermal perturbation.

This work represents the first published application of the CLN package or BHE simulation and in future some improvements and in-depth analysis should be done in order to refine the package capacity to fully represent the involved heat transport mechanisms. The CLN approach does not consider the convective heat transfer coefficient, but when the simulations aim is the environmental impact, neglecting this coefficient does not lead to wrong results. Indeed, the inclusion of this mechanism would improve the capacity of CLN to simulate the BHE energy performances and the outlet fluid temperatures with a greater accuracy.

Furthermore, an additional validation through experimental data (e.g. TRT) would allow another step in the CLN package reliability assessment. Even if at present is not possible to simulate a constant heat rate test through the CLN package, this option is presently under implementation and will be available for additional investigations.

CRediT authorship contribution statement

Matteo Antelmi: Resources, Methodology, Software, Validation, Investigation, Data curation, Writing - original draft, Supervision. **Luca Alberti:** Methodology, Writing - review & editing, Supervision, Project administration. **Sara Barbieri:** Software, Validation, Investigation, Data curation, Writing - original draft, Visualization. **Sorab Panday:** Writing - review & editing.

Declaration of Competing Interest

The authors declare that they have no known competing financial interests or personal relationships that could have appeared to influence the work reported in this paper.

References

- Al-Khoury, R., Kölbel, T., Schramedei, R., 2010. Efficient numerical modeling of borehole heat exchangers. *Comput. Geosci.* 36, 1301–1315. <https://doi.org/10.1016/j.cageo.2009.12.010>.
- Alberti, L., Angelotti, A., Antelmi, M., La Licata, I., 2017. A numerical study on the impact of grouting material on borehole heat exchangers performance in aquifers. *Energies* 10. <https://doi.org/10.3390/en10050703>.
- Alcaraz, M., García-Gil, A., Vázquez-Suñé, E., Velasco, V., 2016. Advection and dispersion heat transport mechanisms in the quantification of shallow geothermal resources and associated environmental impacts. *Sci. Total Environ.* 543, 536–546. <https://doi.org/10.1016/j.scitotenv.2015.11.022>.
- Angelotti, A., Alberti, L., La Licata, I., Antelmi, M., 2014a. Energy performance and thermal impact of a Borehole Heat Exchanger in a sandy aquifer: Influence of the groundwater velocity. *Energy Convers. Manag.* 77, 700–708. <https://doi.org/10.1016/j.enconman.2013.10.018>.
- Angelotti, A., Alberti, L., La Licata, I., Antelmi, M., 2014b. Borehole heat exchangers: Heat transfer simulation in the presence of a groundwater flow. *J. Phys. Conf. Ser.* 501. <https://doi.org/10.1088/1742-6596/501/1/012033>.
- Antelmi, M., 2016. Modellazione numerica del trasporto di calore in falda per lo studio delle prestazioni energetiche e degli impatti termici derivanti dall'attività di una sonda geotermica (in Italian). PHD Thesis 1–282.
- Antelmi, M., Alberti, L., Angelotti, A., Curnis, S., Zille, A., Colombo, L., 2020. Thermal and hydrogeological aquifers characterization by coupling depth-resolved thermal response test with moving line source analysis. *Energy Convers. Manag.* 225, 113400. <https://doi.org/10.1016/j.enconman.2020.113400>.
- Arning, E., Kölling, M., Panteleit, B., Reichling, J., Schulz, D.H.D., 2006. Einfluss oberflächennaher Wärmegewinnung auf geochemische Prozesse im Grundwasserleiter. *Grundwasser* 11, 27–39. <https://doi.org/10.1007/s00767-006-0116-0>.
- Barbieri, S., 2020. Adattamento del pacchetto Connected Linear Network per la modellazione numerica di scambiatori geotermici in MODFLOW-USG. Master Degree Thesis 1–168.
- Bauer, D., Heidemann, W., Diersch, H.J.G., 2011. Transient 3D analysis of borehole heat exchanger modeling. *Geothermics* 40, 250–260. <https://doi.org/10.1016/j.geothermics.2011.08.001>.
- Bonte, M., Stuyfzand, P.J., Van Den Berg, G.A., Hijnen, W.A.M., 2011. Effects of aquifer thermal energy storage on groundwater quality and the consequences for drinking water production: A case study from the Netherlands. *Water Sci. Technol.* 63, 1922–1931. <https://doi.org/10.2166/wst.2011.189>.
- Brunetti, G., Saito, H., Saito, T., Šimůnek, J., 2017. A computationally efficient pseudo-3D model for the numerical analysis of borehole heat exchangers. *Appl. Energy* 208, 1113–1127. <https://doi.org/10.1016/j.apenergy.2017.09.042>.
- Capozza, A., De Carli, M., Zarrella, A., 2013. Investigations on the influence of aquifers on the ground temperature in ground-source heat pump operation. *Appl. Energy* 107, 350–363. <https://doi.org/10.1016/j.apenergy.2013.02.043>.
- Casasso, A., Sethi, R., 2019. Assessment and minimization of potential environmental impacts of ground source heat. *Water (Switzerland)* 1–19.
- Casasso, A., Sethi, R., 2014. Efficiency of closed loop geothermal heat pumps: A sensitivity analysis. *Renew. Energy* 62, 737–746. <https://doi.org/10.1016/j.renene.2013.08.019>.
- Choi, J.C., Lee, S.R., Lee, D.S., 2011. Numerical simulation of vertical ground heat exchangers: Intermittent operation in unsaturated soil conditions. *Comput. Geotech.* 38, 949–958. <https://doi.org/10.1016/j.compgeo.2011.07.004>.
- Diersch, H.J.G., Bauer, D., Heidemann, W., Rühaak, W., Schätzl, P., 2011a. Finite element modeling of borehole heat exchanger systems. Part 1 Fundamentals. *Comput. Geosci.* 37, 1122–1135. <https://doi.org/10.1016/j.cageo.2010.08.003>.
- Diersch, H.J.G., Bauer, D., Heidemann, W., Rühaak, W., Schätzl, P., 2011b. Finite element modeling of borehole heat exchanger systems. Part 2. Numerical simulation. *Comput. Geosci.* 37, 1136–1147. <https://doi.org/10.1016/j.cageo.2010.08.002>.
- Diersch, H.J.G., Bauer, D., Heidemann, W., Rühaak, W., Schätzl, P., 2010. FEFLOW 6.1 - Finite element subsurface flow & transport simulation system. DHI-Wasy SoftwUser Man. 104.
- Epting, J., García-Gil, A., Huggenberger, P., Vázquez-Suñé, E., Mueller, M.H., 2017. Development of concepts for the management of thermal resources in urban areas – Assessment of transferability from the Basel (Switzerland) and Zaragoza (Spain) case studies. *J. Hydrol.* 548, 697–715. <https://doi.org/10.1016/j.jhydrol.2017.03.057>.
- Epting, J., Händel, F., Huggenberger, P., 2013. Thermal management of an unconsolidated shallow urban groundwater body. *Hydrol. Earth Syst. Sci.* 17, 1851–1869. <https://doi.org/10.5194/hess-17-1851-2013>.
- Feinstein, D.T., Fienen, M.N., Reeves, H.W., Langevin, C.D., 2016. A semi-structured MODFLOW-USG model to evaluate local water sources to wells for decision support. *Groundwater* 54, 532–544. <https://doi.org/10.1111/gwat.12389>.
- Ferguson, G., Woodbury, A.D., 2004. Subsurface heat flow in an urban environment. *J. Geophys. Res. Solid Earth* 109, 1–9. <https://doi.org/10.1029/2003jb002715>.
- Floreac, L.J., Hart, D., Tinjum, J., Choi, C., 2017. Potential impacts to groundwater from ground-coupled geothermal heat pumps in district scale. *Groundwater* 55, 8–9. <https://doi.org/10.1111/gwat.12484>.
- Guimerà, J., Ortuno, F., Ruiz, E., Delos, A., Pérez-Paricio, A., 2007. Influence of ground-source heat pumps on groundwater. *Proc. Eur. Geotherm. Congr.* 1–8.
- Hähnlein, S., Bayer, P., Ferguson, G., Blum, P., 2013. Sustainability and policy for the thermal use of shallow geothermal energy. *Energy Policy* 59, 914–925. <https://doi.org/10.1016/j.enpol.2013.04.040>.
- Hancock, P.J., Hunt, R.J., Boulton, A.J., 2009. Preface: Hydrogeoecology, the interdisciplinary study of groundwater dependent ecosystems. *Hydrogeol. J.* 17, 1–3. <https://doi.org/10.1007/s10040-008-0409-8>.
- Harbaugh, A.W. 2005. MODFLOW-2005, The U.S. Geological Survey Modular Ground-Water Model — the Ground-Water Flow Process. U.S. Geol. Surv. Tech. Methods 253. <https://doi.org/U.S. Geological Survey Techniques and Methods 6-A16>.
- Harbaugh, A.W., Banta, E.R., Hill, M.C., McDonald, M.G., 2000. MODFLOW-2000, The U.S. Geological Survey modular ground-water model — User guide to modularization concepts and the ground-water flow process. U.S. Geol. Surv. 130.
- Kupfersberger, H., Rock, G., Draxler, J.C., 2017. Inferring near surface soil temperature time series from different land uses to quantify the variation of heat fluxes into a shallow aquifer in Austria. *J. Hydrol.* 552, 564–577. <https://doi.org/10.1016/j.jhydrol.2017.07.030>.
- Langevin, C.D., Dausman, A.M., Sukop, M.C., 2010. Solute and heat transport model of the Henry and Hilleke laboratory experiment. *Groundwater* 48, 757–770. <https://doi.org/10.1111/j.1745-6584.2009.00596.x>.
- Lee, J.Y., Hahn, J.S., 2006. Characterization of groundwater temperature obtained from the Korean national groundwater monitoring stations: Implications for heat pumps. *J. Hydrol.* 329, 514–526. <https://doi.org/10.1016/j.jhydrol.2006.03.007>.
- Ly, F. 2015. Interpretation of Borehole Heat Exchangers Thermal Response Tests under groundwater influence: analysis of three case studies. Master Degree Thesis.
- Menberg, K., Bayer, P., Zosseeder, K., Rumohr, S., Blum, P., 2013. Subsurface urban heat islands in German cities. *Sci. Total Environ.* 442, 123–133. <https://doi.org/10.1016/j.scitotenv.2012.10.043>.
- Molina-Giraldo, N., Blum, P., Zhu, K., Bayer, P., Fang, Z., 2011. A moving finite line source model to simulate borehole heat exchangers with groundwater advection. *Int. J. Therm. Sci.* 50, 2506–2513. <https://doi.org/10.1016/j.ijthermalsci.2011.06.012>.
- Neville, C.J., Tonkin, M.J., 2004. Modeling multiaquifer wells with MODFLOW. *Ground Water* 42, 910–919. <https://doi.org/10.1111/j.1745-6584.2004.t01-9-x>.
- Niswonger, R.G., Panday, S., Ibaraki, M., 2011. MODFLOW-NWT, A Newton Formulation for MODFLOW-2005. *Groundw. B*, 6, Sect. A, Model. Tech. Book 6-A37, 44.
- Panday, S., 2020. USG-Transport Version 1.5.0: The Block-Centered Transport (BCT) Process for MODFLOW-USG.
- Panday, S., Langevin, C.D., Niswonger, R.G., Ibaraki, M., Hughes, J.D., 2013. MODFLOW – USG version 1: An unstructured grid version of MODFLOW for simulating groundwater flow and tightly coupled processes using a control volume finite-difference formulation. *U.S. Geol. Surv.* 66.
- Piccinini, L., Vincenzi, V., Pontin, A., Tonet, F., 2012. Technical report Modello di trasporto di calore per il dimensionamento di un sistema di geoscambio a circuito aperto. *Ital. J. Groundw.* 67–79. <https://doi.org/10.7343/AS-011-12-0030>.
- Riedel, T., 2019. Temperature-associated changes in groundwater quality. *J. Hydrol.* 572, 206–212. <https://doi.org/10.1016/j.jhydrol.2019.02.059>.

- Sbai, M.A., 2020. Unstructured gridding for MODFLOW from Prior groundwater flow models: A new paradigm. *Groundwater*. <https://doi.org/10.1111/gwat.13025>.
- Šimůnek, J., van Genuchten, M.T., Šejna, M. 2016. Recent Developments and Applications of the HYDRUS Computer Software Packages. *Vadose Zo.* J. 15, vj2016.04.0033. <https://doi.org/10.2136/vj2016.04.0033>.
- Somogyi, V., Sebestyén, V., Domokos, E., Zseni, A., Papp, Z., 2015. Thermal impact assessment with hydrodynamics and transport modeling. *Energy Convers. Manag.* 104, 127–134. <https://doi.org/10.1016/j.enconman.2015.04.045>.
- Taylor, C.A., Stefan, H.G., 2009. Shallow groundwater temperature response to climate change and urbanization. *J. Hydrol.* 375, 601–612. <https://doi.org/10.1016/j.jhydrol.2009.07.009>.
- Thorne, D., Langevin, C.D., Sukop, M.C., 2006. Addition of simultaneous heat and solute transport and variable fluid viscosity to SEAWAT. *Comput. Geosci.* 32, 1758–1768. <https://doi.org/10.1016/j.cageo.2006.04.005>.
- Zanchini, E., Lazzari, S., Priarone, A., 2012. Long-term performance of large borehole heat exchanger fields with unbalanced seasonal loads and groundwater flow. *Energy* 38, 66–77. <https://doi.org/10.1016/j.energy.2011.12.038>.
- Zheng, C., Wang, P.P., 1999. MT3DMS: A Modular three-dimensional multispecies transport model for simulation of advection, dispersion and chemical reactions of contaminants in groundwater systems. *Contract Rep. SERDP-99-1*, 239.